10.21611/qirt.2023.11

QIRT Asia 2023

4th Asian Quantitative InfraRed Thermography Conference

Numerical modelling and experimental approach for defect detection in CFRP by microwave thermography

by F. Brachelet*, S. Keo**[1,2], B. Szymanik***, C. Le Roy**** and D.Defer*

* Univ. Artois, IMT Nord Europe, Junia, Univ. Lille, ULR 4515, Laboratoire de Génie Civil et géo-Environnement (LGCgE), F-62400 Béthune, France,
franck.brachelet@univ-artois.fr , didier.defer@univ-artois.fr
**[1] *Cerema, Research Team ENDSUM, 23 Amiral Chauvin Avenue, 49130 Les Ponts-de-Cé, France*
**[2] *École Spéciale des Travaux Publics, du Bâtiment et de l'Industrie, Campus métropolitain – 9-11 rue Sully – 21 000 Dijon, France,* sakeo@estp-paris.eu
*** Center for Electromagnetic Fields Engineering and High-Frequency Techniques, Faculty of Electrical Engineering, West Pomeranian University of Technology, Szczecin, Poland, szymanik@zut.edu.pl
**** Independent Researcher, Sikorski St. 37, 70-313 Szczecin, Poland, claire29370@yahoo.fr

Abstract

This paper describes the application of infrared thermography combined with microwave excitation to detect bonding defects in a carbon fiber reinforced concrete structure. Electromagnetic and thermal phenomena are modelled and compared with experiment. Several short-term tests have been carried out, using both continuous and pulsed excitations, and showed that detection of this type of defect was possible.

1. Introduction

Reinforcing concrete structures with Carbon Fiber Reinforced Polymer (CRFP) is a technique that is gradually gaining ground around the world. In many case, the application of CFRP reinforcement typically involves the adhesion of an epoxy resin-bonded layer composed of multiple carbon mats onto the cement substrate. The lack of adhesive or the occurrence of delamination results in local reduction in the strength of the reinforcement, thereby creating a weak area favourable for potential harm of the construction [1]. Consequently, it is of utmost significance to control said structures with regards to evaluating the quality of the bond between concrete and composite. Various non-destructive testing techniques can be employed to monitor the quality of the cement-composite joint. The present paper aims to study the active thermography technique with microwave excitation (MWT) applied to the defect detection in the CFRC samples.

Active thermography involves the use of an external energy source in order to generate heat diffusion within the sample under test. [2]. In this proposal, microwaves are suggested as a potential energy source for infrared thermography [3]. The primary benefit of utilizing microwave heating lies in its volumetric nature. The first studies combining infrared thermography and electromagnetic waves date from the early 90s [4]. The EMIR method aims to characterize the radiation patterns of antennas using an infrared camera. In this method, a photothermal thin films is used to convert the Electromagnetic field into a thermal map which is detected with an infrared camera. In subsequent articles [4], authors describe the differences in sensitivity of the method depending on whether the incident waves are continuous or modulated. The rapidity of this technique is attributed to the heating of a specific volume of the specimen at a given time. An interesting phenomenon is observed when microwaves interact with conductive materials, such as reinforcement bars [6-8] or CFRP [9]. The heating effect is constrained by a lower penetration depth value. Following the application of heat, an infrared camera records the surface temperatures of the specimen under inspection. Non-uniform heating of a sample can be attributed to the presence of inner material flaws such as delamination and lack of adhesive. These flaws result in the manifestation of hotter or cooler regions visible in the temperature distribution on the sample's surface.

2. Numerical Modeling

The numerical model presented in this study was developed within the commercial software platform COMSOL. The Finite Element Method (FEM) was employed to perform the calculations. The modelling of Microwave Thermography (MWT) necessitates the examination of two phenomena in a multi-physics mode, namely electromagnetic wave propagation (EMW) and heat transfer (HT). The calculations were performed in the frequency (for EMW) and time domains (HT) for continuous excitation and in the time domain for modulated excitation.

The present study aims to examine the feasibility of utilizing active microwave thermography as a means of investigating reinforced concrete structures that have been strengthened with carbon fiber reinforced polymer (CFRP). At the outset, a numerical model was developed to analyse the phenomenon being investigated. The objective of the model

was to replicate the laboratory configuration and to examine scenarios that were not executed in the experiment, with the aim of assessing the applicability of the approach in a wider context. Consequently, we constructed models that depict the sample's heating in both modulated (mirroring the experimental approach) and continuous modes. Furthermore, a defect-free sample and a centrally located defective sample were simulated, as per the experimental conditions. Additionally, a scenario was considered where the defect is not centrally located. Section 2 presents a numerical model along with illustrative outcomes for each scenario.

2.1. Model geometry

A pyramid-shaped horn antenna was used to broadcast the waves to the samples under test. The dimensions of the antenna's aperture were 590 mm x 560 mm, while its height measured 660 mm. The antenna was connected to a rectangular waveguide that had dimensions of 36 mm x 62 mm and a length of 150 mm. The geometry was import in the COMSOL software.

A concrete slab, which dimensions 400 mm x 400 mm x 45 mm, reinforced with CFRP, was used to model the test sample. The composite reinforcement was represented as a bilayer structure comprising an epoxy adhesive layer measuring 1 mm in thickness and a layer of CFRP composite with a thickness of 1 mm. The defect in a form of a lack of adhesive was represented as a void space within the layer of epoxy adhesive. The dimensions of the defect were 100 mm x 100 mm, and 1 mm in height. Three cases were simulated, namely: defect-free, centrally-located defect, and off-center defect.

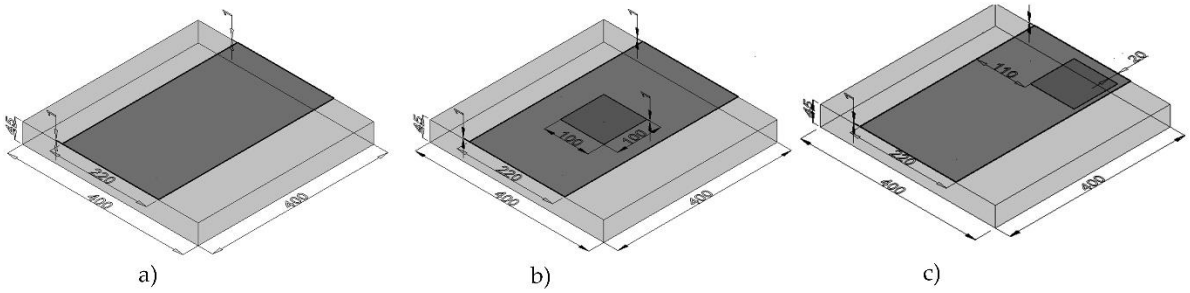

Fig. 1. *Models of the samples: (a) case without the defect, (b) case with the defect located in the center of the sample, and (c) case with the defect located away from the centre of the sample (dimensions in mm)*

2.2. Boundary conditions and material properties and meshing

The specimen was positioned at a distance of 200 mm from the central point of the antenna aperture and was rotated at an angle of 45° with respect to main direction of the antenna. Figure 2 (a) shows the full geometry of the model. In order to minimize the calculation time and the necessary computational resources, the simulation covered only 1/2 of the model. The mesh is shown on the left side in figure 2. It is based of 76,093 tetrahedral elements in the case without defects, 79,677 elements in the case with a defect area located in the center of the sample, and 80,049 in the case with a defect area located outside the center. As it can be notice, the size of the elements changes depending on the domains.

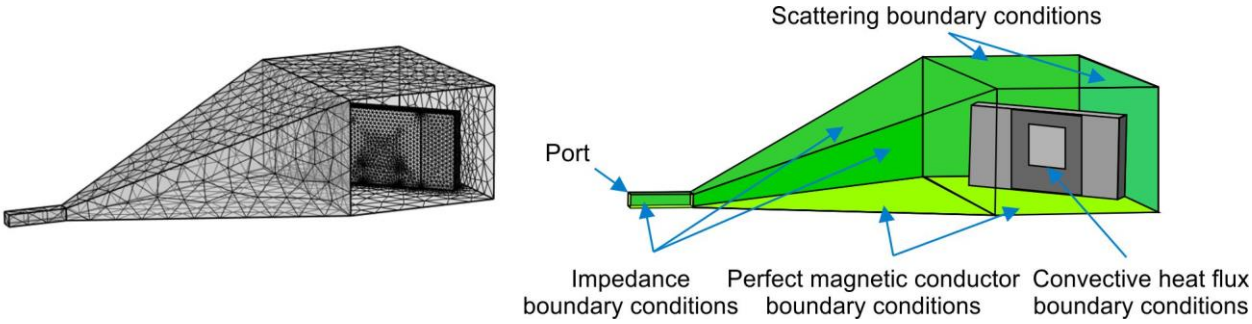

Fig. 2. *(a) Mesh of the model – (b) Specification of the boundary conditions*

The specified boundary conditions are presented on the right side in figure 2 (b). The model was computed in two modes: continuous (with an equal power of 360 W applied for all the time of simulation) and modulated with the power applied with a function f(t) presented in figure 3:

$$P_{mod} = 360[w] \cdot f(t)$$

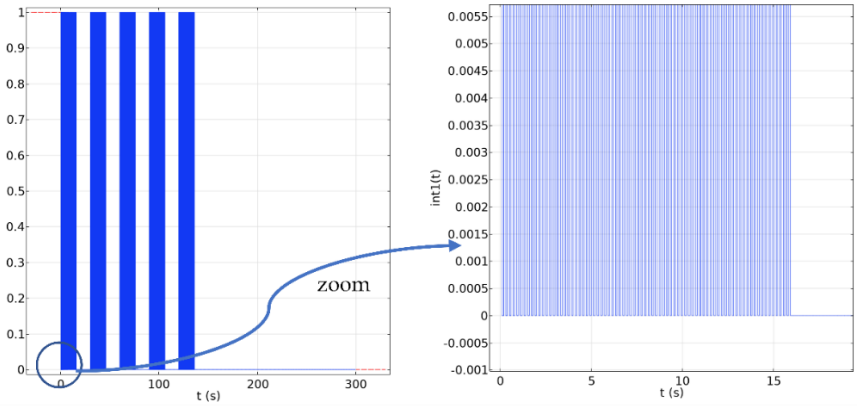

Fig. 3. *Power modulated by a rectangular waveform*

The table 1 presents selected properties of the materials used in the simulation.

	Air	Aluminium	Epoxy	GRFP	Concrete
Cp [J/(kg.K)]		N/A	1700	1700	750
Density [kg/m^3]		N/A	1150	1150	2400
ε relative permittivity	1	1	3.9-2.2j	3.6	8.4-2.86j
λ Thermal conductivity [W/(m.K)]		N/A	0.18	5	0.8
σ Electrical conductivity [S/m]	0	3.77e7	0	0.5	0
μ relative permeability	1	1	1	1	1

Table 1. *Material parameters*

As previously stated, the modelling of microwave heating necessitates a comprehensive examination of the issue through a combination of two distinct fields of physics: electromagnetic wave propagation and heat transfer. The model presented in this study described the propagation of an electromagnetic wave through the utilization of the electromagnetic wave equation, specifically in the frequency domain:

$$\nabla^2 \vec{E} + \left(p\varepsilon w^2 - i\mu\sigma w \right) \vec{E} = 0 \tag{1}$$

where μ denotes the magnetic permeability, ϵ is the electric permittivity, σ represents the electric conductivity, ω is the angular frequency, and $\vec{E}$ is the electric field vector. This equation is solved in all domains within the model. Conversely, the heat transfer was characterized by the heat balance equation defined as follows:

$$\rho C_p \left(\frac{\partial T}{\partial t} + \nabla T \right) + \nabla \vec{q} = Q \tag{2}$$

where ρ is the material density, C_p denotes the material heat capacity, q is the heat flux associated with the convection phenomenon, T is the temperature, and Q denotes the external heat source. This phenomenon was exclusively taken into account within domains that were associated with the sample. The external heat source was equal to the resistive heat generated by the electromagnetic field, which is described as follows (derived from Poynting's theorem):

$$Q = \frac{1}{2} \Re e \left((\sigma - j\omega\varepsilon) \vec{E} . \vec{E^*} \right) \tag{3}$$

where Re indicates the real part of the value. Accurately simulating the phenomenon under investigation necessitates the identification of suitable boundary conditions for both electromagnetic waves and heat transfer. The simulated antenna's walls were subjected to an impedance boundary condition, which is defined as follows:

$$\sqrt{\frac{\mu}{\varepsilon - j\sigma/\omega}}\,\vec{n}\times\vec{H}=\vec{n}\times\vec{E} \tag{4}$$

where $\vec{H}$ is the magnetic field strength vector and $\vec{n}$. The walls of the air-filled domain surrounding the sample were subjected to a scattering boundary condition [47]:

$$\vec{n}\times\left(\vec{\nabla}\times\vec{E}\right)-jk\vec{n}\times(\vec{E}\times\vec{n})=0 \tag{5}$$

where k is the wavenumber. An electromagnetic wave was produced through the application of the port boundary condition on a specific wall within the waveguide. Here, the assumed mode was TE_{10} and the propagation constant was equal to :

$$\beta=\frac{\omega}{c}\sqrt{1-\frac{\omega_c^2}{\omega^2}} \tag{6}$$

Where $\omega_c=c\sqrt{\left(\frac{n\omega}{a}\right)^2-\left(\frac{m\omega}{b}\right)^2}$ is the cut-off frequency of a waveguide, where n = 1 and m = 0.

Finally: $$\beta=\frac{2\pi}{c}\sqrt{f^2-\frac{c^2}{4a^2}} \tag{7}$$

where a = 62 mm was the width of the rectangular waveguide, c denotes the speed of light, and f denotes the frequency. The perfect magnetic conductor condition was imposed on the plane of symmetry, which served to define the division of the model:

$$\vec{n}\times\vec{H}=0 \tag{8}$$

Regarding the HT domain, which was confined solely within the sample, the convective flux condition was enforced on all walls of this domain as the boundary condition:

$$q_c=h\left(T_{ext}-T\right) \tag{9}$$

where h denotes the heat transfer coefficient and T_{ext} is the external temperature value.

2.3. Simulation results

The following section provides a broader overview of the results. The presented figures 4 depict thermograms that were selectively chosen for both continuous on the left and modulated excitation on the right. The complete thermograms of the sample, both without a defect and with a centrally located defect, was reconstructed through mirror reflection (figures 4 a&b). It should be noted that in the case of a system featuring an off-centre defect, the aforementioned operation was not feasible. Consequently, in this case, we solely present one-half of the surface, as it was simulated in COMSOL (figures 4 c). The results of the study are shown in the form of unprocessed temperature distributions, namely, thermograms, in which the temperature values were standardized to a singular temperature scale. The outcomes for three specific time intervals are demonstrated, namely, at 50 s, 100 s, and 150 s, which corresponded to the end of the heating process. The data indicate that the temperature under continuous excitation was notably higher compared with that under modulated excitation, with maximum values of 18.88 °C and 16.11 °C, respectively. However, it is noteworthy that in both instances, the defect became apparent at the 50 s mark and the qualitative outcomes were similar. For instances of continuous heating, the central region of the sample experienced a considerably higher degree of heating compared with its off-centre counterpart. This is a crucial factor to consider when the defect is located away from the centre. The enhanced detectability of the off-centre defect under modulated excitation was readily apparent.

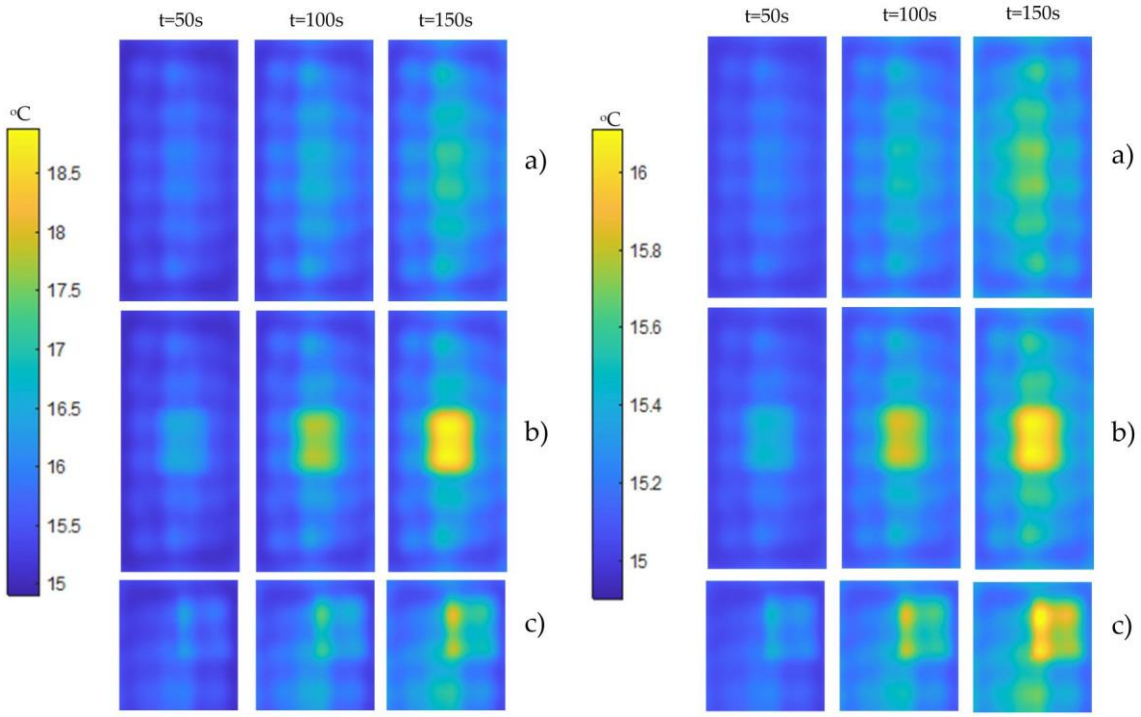

Fig. 4. *Simulation results for continuous excitation and modulated excitation*

3. Experimental tests and Results

3.1. Sample and experimental setup

Two experimental campaigns were carried out: one with a CFRP sample without a defect and another test with a sample with a defect, which corresponded to two cases of the numerical simulations (defect-free and a centrally located defect, respectively). Figure 5 below shows carbon fiber reinforced concrete slab used in the study. The adhesive was Araldite® 2015, which is a two-component epoxy paste adhesive, particularly suitable for SMC and GRP bonding. The carbon fibers are the SikaWrap®-301 C. The composite laminate was defined as the stacking of two uni-directional plies with two different fibers orientations (perpendicular). The defect was represented by the presence of air (the absence of an epoxy adhesive layer with a thickness of 1 mm) over an area of 100 mm × 100 mm.

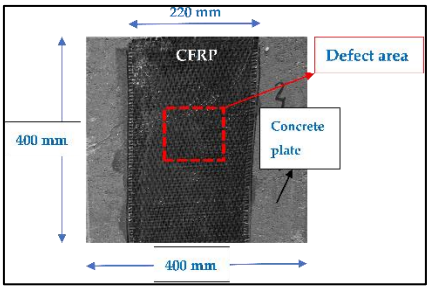

Fig. 5. *Carbon fiber reinforced sample*

The experimental setup of the tests with the CFRP samples is shown in figure 5. The microwave system used to stimulate the samples is the same as for the numerical model. The generator is a magnetron operating at a 2.45 GHz frequency. The pyramidal horn antenna is placed at the same position and in the same direction as in the numerical model (200 mm from the sample and with a 45° direction). A heating power of 360 W is used for heating the samples for 150 s. In order to record the surface temperatures of the heated specimen for comparison with the numerical model, the temperatures recordings have been performed by a cooled infrared camera, Silver 420M model from CEDIP company. It is equipped with 320 x 256 pixels InSb array sensitives to mid-infrared radiation between 3 and 5 µm and presents thermal

sensitivity (NETD) < 30 mK. Moreover, in order to detect the whole surface of the specimen, the following position of the infrared camera was chosen: 55° direction with a distance of 1.5 m from the sample. The thermograms were recorded at a frame rate of 1 image per second and for a duration of 475 s in order to observe the cooling phase of the experiments.

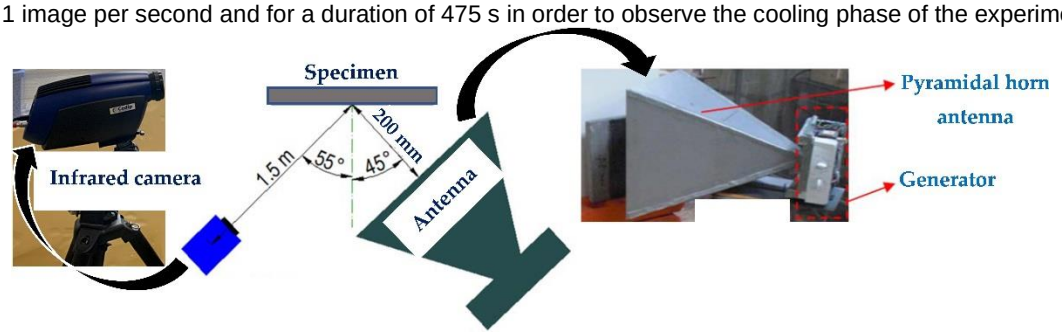

Fig. 5. *Experimental test setup with CFRP and*

3.2. Results from experimental campaigns

The thermograms are compared to those obtained with the numerical simulation at the same times, i.e., 50 s, 100 s and 150 s. Thermograms in figure 6, show that the defective area has a higher temperature rise than the sound, well-bonded area. That higher rise in temperature over the defected area is explained by the underlying presence of an air gap whose thermal conductivity is lower than that of the epoxy resin. Furthermore, we also observe a non-uniformity of the dissipated heat due to the non-uniformity of the microwave beams. The appearance of these additional zones is in accordance with the simulation.

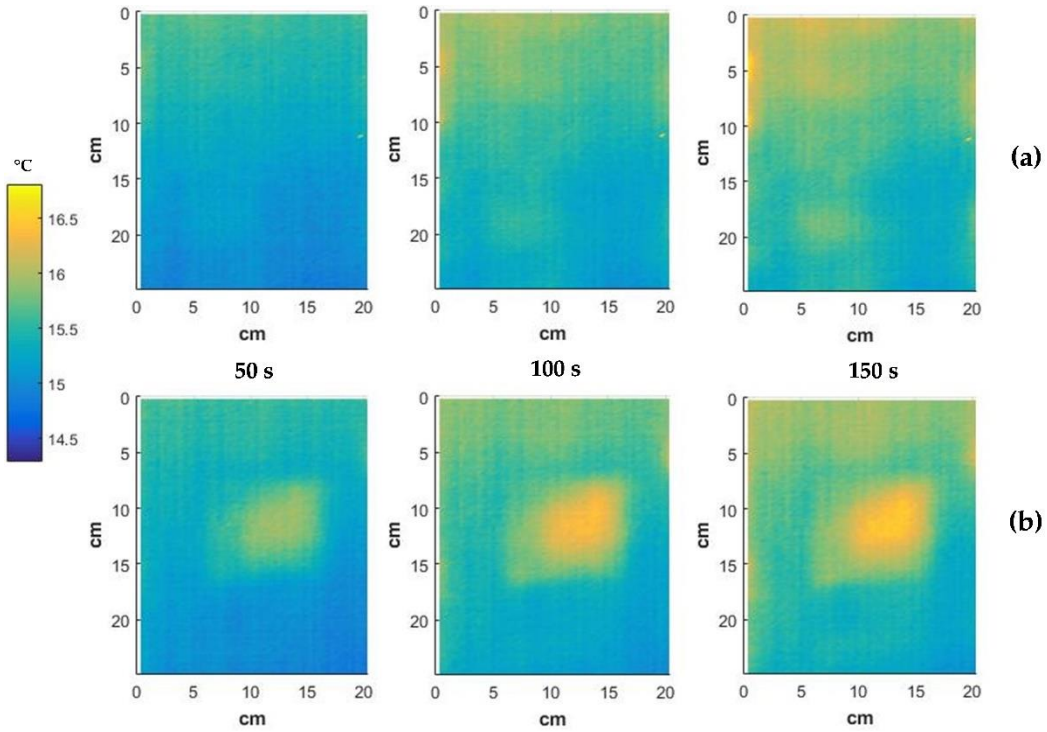

Fig. 6 Experimental thermograms of the test slabs

The temporal evolutions of the temperature on the defect and non-defect regions for both samples are shown in figure 7. In accordance with the results from the numerical modelling, the temperature curves clearly show modulation due to the microwave signal excitation. After the heating phase (150 s), the modulation disappeared from the temperature curves. In the defect area (red solid curve), the temperature increased from 15.2 °C to 16.2 °C, while that of the defect-

free region (blue dotted curve) increased only from 14.9 °C to 15.3 °C (figure 7b). On the other hand, there was only a small difference between both observed regions on the sample without a defect (both curves in figure 7a), although there was an effect of the non-uniformity of the microwave beam.

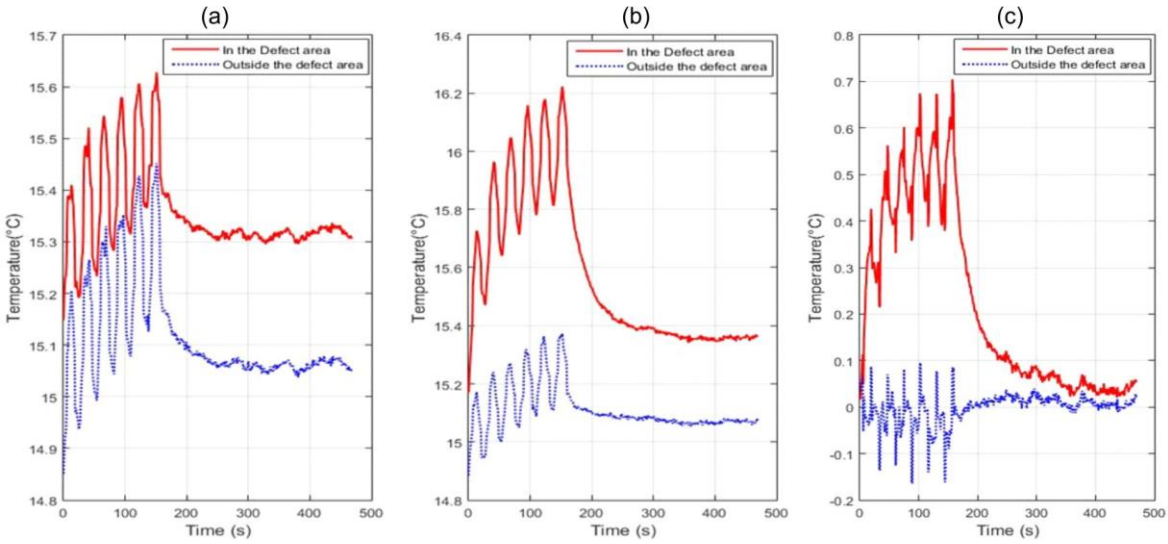

Fig. 7 Time–temperature characteristics obtained for both samples: (a) sample without a controlled defect and (b) sample with a controlled defect, (c) Temperatures differences between (a) and (b)

The temporal evolutions of the temperatures between both samples can be also observed in figures 7 (a) & (b). As both samples may have had different surface temperatures at the beginning of the test, the initial temperatures were subtracted from the temperature evolutions. Obviously, the maximal temperature difference (0.7 ℃) is at the end of the heating phase. It is important to notice that the comparison between the experimental approach and the numerical modelling, especially the results with the modulated excitation, show a higher temperature at the defect area than the area without a defect. Another common point of the results from both approaches is the influence of the non-uniformity of the microwave beam on the thermograms. This non-uniformity is generated by the reflection of the waves between the antenna and the sample. This phenomenon must be considered in this detection using MWT method.

4. Conclusion

In the present study, the feasibility of using MWT for monitoring reinforced concrete structures strengthened with CFRP has been examined. The compliance of the results from both numerical and experimental approaches in the case of a modulated excitation allowed to validate the numerical model for detecting defect in CFRP. The defect area, which was represented by the absence of adhesive or the presence of the air, had higher surface temperature than the temperature of the area without defect. The common results from both approaches also lead to highlight the non-uniformity of the microwave beam, a phenomenon having to be considered because it can enable to misinterpret the thermograms for deducing the defects. Besides the validation of the numerical model with the experimental campaign, the wider context of the study was also given by the numerical model: position of the defect, and the rapidity of the method by using the modulated excitation compared to the continuous excitation.

REFERENCES

[1] Shang, X.; Marques, E.A.S.; Machado, J.J.M.; Carbas, R.J.C.; Jiang, D.; Silva, L.F.M. da. Review on Techniques to Improve the Strength of Adhesive Joints with Composite Adherends. Compos. Part B Eng. 2019, 177, 107363. https://doi.org/10.1016/j.compositesb.2019.107363.

[2] Maldague, X.P.V. Theory and Practice of Infrared Technology for Nondestructive Testing; Wiley series in microwave and optical engineering; Wiley: New York, NY, USA, 2001.

[3] Balageas D., Levesque P., EMIR: a photothermal tool for electromagnetic phenomena characterization", September 1998, Revue Générale de Thermique 37(8):725-739, DOI: 10.1016/S0035-3159(98)80050-0

[4] Levesque P., Brémond P., J.-L. Lasserre, Paupert A., Balageas D. L. “Performance of FPA IR cameras and of their improvement by time, space and frequency data processing. Part II - Application to the thermographic measurement of microwave fields”, Quantitative InfraRed Thermography Journal. - Vol. 2, no 2 (2005), pp. 237-250, 2005. DOI:10.3166/qirt.2.237-250.
[5] Keo, S. A.; Brachelet, F.; Breaban, F.; Defer, D. Steel Detection in Reinforced Concrete Wall by Microwave Infrared Thermography. NDT & E International. 2014, 62, 172–177. https://doi.org/10.1016/j.ndteint.2013.12.002.
[6] Brachelet F., Keo S., Defer D., Breaban F., Detection of reinforcement bars in concrete slab by infrared thermography and microwaves excitation, 12th International Conference on Quantitative Infrared Thermography, France, Bordeaux, 7 - 11 July 2014 (QIRT 2014).
[7] Szymanik, B.; Frankowski, P.; Chady, T.; John Chelliah, C. Detection and Inspection of Steel Bars in Reinforced Concrete Structures Using Active Infrared Thermography with Microwave Excitation and Eddy Current Sensors. Sensors. 2016, 16 (2), 234. https://doi.org/10.3390/s16020234.
[8] Galietti U., Palumbo D., Calia G. and Ancona F., “New data analysis to evaluate defects in composite materials using microwaves thermography”. 11th International Conference on Quantitative InfraRed Thermography (QIRT 2012), Naples, Italy, 11-14 Jun 2012. paper 2012-10, DOI: 10.21611/qirt.2012.249.
[9] COMSOL Multiphysics® v. 6.1. www.comsol.com. COMSOL AB, Stockholm, Sweden.